

Enhancing Protein-Ligand Binding Affinity Predictions using Neural Network Potentials

Francesc Sabanés Zariquiey,^{†,‡} Raimondas Galvelis,^{†,‡} Emilio Gallicchio,[¶] John D. Chodera,[§] Thomas E. Markland,^{||} and Gianni De Fabritiis^{*,†,‡,⊥}

[†]*Computational Science Laboratory, Universitat Pompeu Fabra, Barcelona Biomedical Research Park (PRBB), C Dr. Aiguader 88, 08003, Barcelona, Spain*

[‡]*Acellera Labs, C Dr Trueta 183, 08005, Barcelona, Spain*

[¶]*Department of Chemistry, Brooklyn College of the City University of New York; PhD Program in Chemistry, Graduate Center of the City University of New York; PhD Program in Biochemistry, Graduate Center of the City University of New York, NY 11210, USA*

[§]*Computational and Systems Biology Program, Sloan Kettering Institute, Memorial Sloan Kettering Cancer Center, New York, NY 10065, USA*

^{||}*Department of Chemistry, Stanford University, 337 Campus Drive, Stanford, CA, 94305, USA*

[⊥]*Institució Catalana de Recerca i Estudis Avançats (ICREA), Passeig Lluís Companys 23, 08010 Barcelona, Spain*

E-mail: g.defabritiis@gmail.com

Abstract

This letter gives results on improving protein-ligand binding affinity predictions based on molecular dynamics simulations using machine learning potentials with a hybrid neural network potential and molecular mechanics methodology (NNP/MM). We compute relative binding free energies (RBFE) with the Alchemical Transfer Method (ATM) and validate its performance against established benchmarks and find significant enhancements compared to conventional MM force fields like GAFF2.

1 Introduction

In modern drug discovery, alchemical free energy calculations have emerged as highly efficient tools. Relative binding free energy calculations are widely employed in hit-to-lead approaches, and several commercial and free tools with comparable performance have been devel-

oped over the years. However, the accuracy of binding free energy calculations is influenced by the choice of ligand force field. Most conventional force fields like GAFF^{1,2}, GenFF^{3,4}, and OPLS⁵ often rely on fixed charge molecular mechanics (MM). This lack of important energetic contributions limits their chemical accuracy and leads to poor modeling of torsions.⁶⁻⁸

To address these limitations, one approach involves using quantum mechanical (QM) levels of theory to model the ligands while treating the remaining environment with an MM force field in a hybrid potential.⁹ However, QM/MM calculations are significantly more computationally expensive than MM calculations, posing challenges for drug discovery settings where RBFE calculations may be required for dozens or even hundreds of ligands. Recently, neural network potentials (NNPs) have shown success in predicting QM energies with significantly reduced computational cost compared to QM methods. Notably, the ANI-2x¹⁰ model supports molecular systems comprising elements

H, C, N, O, S, F, and Cl. Moreover, a hybrid method that integrates NNPs and MM, known as NNP/MM¹¹, has been developed, offering the potential to model ligands more accurately in RBFE calculations than traditional MM force fields. The Alchemical Transfer Method (ATM) is a recently developed methodology for alchemical free energy calculations that we recently validated that allows an easy implementation of NNPs¹². In previous publications, this methodology with MM force fields on a robust dataset obtained similar results to other state-of-the-art methods such as FEP+. ^{13,14} In this work, we exploit the capabilities of ATM to test the hybrid approach of using ANI-2x¹⁰ as the neural network potential. Rufa et al. previously managed to reduce the error of absolute binding free energies from 0.97 to 0.47 kcal/mol for a congeneric ligand series for tyrosine kinase TYK2 by correcting the conventional MM simulation with an NNP/MM approach. ¹⁵ ANI-2x has several limitations in terms of non-supporting charged molecules and certain elements but it is otherwise a useful test potential. Our main objective is to test the applicability of this methodology with different ligand force fields and to evaluate the feasibility of an NNP/MM approach in relative binding free energy calculations.

2 Methods

In this study, we evaluated a series of targets from both Wang’s *et al.*¹⁶ and Schindler’s datasets.¹⁷ Due to the limitations of ANI-2x,¹⁰ the NNP of our choice in this study, there is a series of targets from the aforementioned datasets that cannot be computed due to the properties of its ligands. Consequently, we evaluated the following targets: Cyclin-dependent kinase 2 (CDK2), c-Jun N-terminal kinase 1 (JNK1), tyrosine kinase 2 (TYK2), P38 MAP kinase (P38), hypoxia-inducible transcription factor 2 (HIF2A), PFKFB3, spleen tyrosine kinase (SYK) and tankyrase 2 (TNKS2), totaling 301 ligand pairs. For the selected targets most of the ligands are compatible with ANI-2x, the rest (and its corresponding lig-

and pair calculations) were removed from the dataset. Due to the higher computational costs related to the integration of NNP into these calculations, a subset of all the possible ligand pairs to be evaluated was selected at random. The workflow in this project is similar to our previous work¹³. Protein and ligand structures were readily available from Wang’s¹⁶ and Schindler’s¹⁷ datasets. Ligands were parameterized with GAFF 2.11^{1,2}. The topologies were generated using the *parameterize*¹⁸ tool. In contrast to our previous work, we now prepared complex systems using HTMD,¹⁹ which automated and streamlined the preparation of multiple ligand pairs, along with the automatic selection of binding site residues. However, the manual selection of atom indexes for ligand alignment remained necessary. The energy minimization, thermalization, and equilibration steps followed the procedures described in our previous work.¹³ Additionally, the system was annealed to the symmetric alchemical intermediate ($\lambda = 1/2$) for 250 ps. The classical RBFE simulations (GAFF2) were run in triplicate for each ligand pair running an ensemble of 60 ns per replica. Concurrently, we performed the same calculations by using an NNP/MM approach.¹¹ This hybrid method allowed us to simulate a portion of the molecular system (the small molecule) with an NNP, while the rest was simulated with MM, providing the ligands with optimized intra-molecular interactions. For both approaches, we used the Amber ff14SB parameters^{20,21} as well as the TIP3P water model. Classical RBFE simulations were run at a 4fs timestep while the NNP/MM runs were computed at 1fs timestep, both with the ATM integrator plugin²². Hamiltonian replica exchange along the λ space for each ATM leg was performed with the ASyncRE software²³, specially customized for OpenMM and ATM.²⁴ Consistent with our previous work, we computed the binding free energies and their corresponding uncertainties from the perturbation energy samples using the Unbinned Weighted Histogram Analysis Method (UWHAM).²⁵ The resulting relative binding free energies ($\Delta\Delta G$) were compared to experimental measurements in terms of mean absolute error (MAE), root

mean square error (RMSE), and Kendall Tau correlation coefficient. For all the possible systems, absolute ΔG values were computed with cinnabar, an analysis tool to compute absolute binding free energies from $\Delta\Delta G$ values via a maximum likelihood estimator.²⁶ Cinnabar also generates the correlation plots and calculates the error and correlation statistics necessary. We compared the obtained values from calculations and the works by Wang *et al*¹⁶ and Schindler *et al*¹⁷ with FEP+. To perform the calculations, we utilized the OpenMM-ML and NNPOps libraries on our in-house cluster comprising NVIDIA RTX 2080 Ti and NVIDIA RTX 4090 cards. Standard MM calculations were run on GPU GRID. The parallel replica exchange molecular dynamics simulations were conducted using the OpenMM 7.7 MD engine and the ATM Meta Force plugin, utilizing the CUDA platform.

3 Results

The results of our simulations are displayed in Table 1 and Figures 1 and 2 which highlight the relative (Kendall’s rank order correlation) and absolute performance (MAE and RMSE) of the evaluated methods. We do not report the Pearson correlation as well because the value is not significant for ($\Delta\Delta G$) values as it varies with the choice of the pairs²⁷. We cannot calculate ΔG for all pairs since we ran a subset of the original datasets. The computation of ΔG for all ligands was not possible due to a poor connection of the perturbation network. Figures S4-S8 displays the ΔG values and related statistics for the systems that were possible to compute. The NNP/MM method demonstrated superior performance over pure MM runs in both relative and absolute measures. We observe that NNP/MM shows a better correlation coefficient and MAE for all of the evaluated systems but PFKFB3 when compared to ATM with GAFF2 as a force field. In comparison to FEP+, NNP/MM has a lower correlation for two systems (P38 and PFKFB3) and higher MAE for four of them (P38, HIF2A, PFKFB3 and TNKS2). Furthermore, the amount of lig-

ands that are more accurately predicted is increased. In comparison to our GAFF2 runs, MM/NNP predicts a higher percentage of ligands with a MAE lower than both 1 and 1.5 kcal/mol.(Table S1). Additionally, there are no major differences between the conformers generated with GAFF2 and ANI-2x as force-fields. (Figure S9) We observe for some specific cases how ligands that participated in poor predictions with GAFF2 (MAE > 2kcal/mol) are now predicted correctly (MAE < 1kcal/mol).(Table S2) However, this improvement comes at a cost, as NNP/MM calculations are slower than conventional MM calculations¹¹. For instance, an RTX 4090 could yield up to 27 ns/day, whereas an ATM conventional run for a P38 system with 49k atoms is able to compute 211 ns/day (Figure S10). This decrease on speed mainly arises due to the limitation of a 1fs timestep with the current ATM integrator. While there is a considerable increase in computational cost for NNP/MM runs, both approaches could benefit from further optimizations. We also evaluate if different timesteps could influence the accuracy of RBFE calculations. We compared the results of the GAFF2 calculations performed in this work with a 4fs timestep with the calculated points from our previous benchmark, that were run at a 2fs timestep.(Figure S11) We do not observe any considerable accuracy difference between the calculations at both timesteps. In terms of convergence, we observed that 60 ns per calculation tends to be sufficient. Convergence analysis over time shows good convergence for most cases as illustrated in Figure S12.

4 Conclusion

We conducted relative binding free energy (RBFE) calculations using an innovative NNP/MM approach. Our findings demonstrate the substantial accuracy enhancement achieved by using an NNP/MM approach at the cost of increased computational time. Compared to conventional ligand forcefields like GAFF2, the NNP/MM approach exhibited reduced mean absolute errors, with most systems reaching be-

Table 1: Comparison of the performance of different forcefields and NNP/MM. Kendall correlation (τ), Mean Absolute Error (MAE) and Root Mean Square Error (RMSE) in kcal/mol for the 8 tested Protein Targets. FEP+ is included as a state-of-the-art comparison.

	GAFF2			NNP/MM ANI2x			FEP+			ligand pairs
	kendall (τ)	MAE	RMSE	kendall (τ)	MAE	RMSE	kendall (τ)	MAE	RMSE	
CDK2	0.42 \pm 0.17	0.8 \pm 0.2	1.1 \pm 0.3	0.62 \pm 0.10	0.7 \pm 0.1	0.8 \pm 0.2	0.42 \pm 0.15	0.8 \pm 0.1	1.1 \pm 0.1	22
JNK1	0.34 \pm 0.14	0.9 \pm 0.2	1.0 \pm 0.2	0.43 \pm 0.12	0.7 \pm 0.1	0.9 \pm 0.2	0.43 \pm 0.14	0.8 \pm 0.1	1.0 \pm 0.1	27
P38	0.48 \pm 0.06	1.2 \pm 0.2	1.6 \pm 0.2	0.59 \pm 0.05	0.9 \pm 0.1	1.2 \pm 0.2	0.60 \pm 0.11	0.8 \pm 0.1	1.0 \pm 0.1	56
TYK2	0.33 \pm 0.15	1.1 \pm 0.2	1.3 \pm 0.3	0.67 \pm 0.10	0.5 \pm 0.1	0.6 \pm 0.1	0.54 \pm 0.15	0.8 \pm 0.2	0.9 \pm 0.1	24
HIF2A	0.43 \pm 0.10	1.6 \pm 0.3	2.0 \pm 0.4	0.55 \pm 0.11	1.3 \pm 0.2	1.6 \pm 0.3	0.50 \pm 0.13	1.1 \pm 0.1	1.3 \pm 0.2	28
PFKFB3	0.49 \pm 0.06	1.3 \pm 0.2	1.6 \pm 0.2	0.37 \pm 0.08	1.3 \pm 0.2	1.7 \pm 0.2	0.70 \pm 0.09	1.0 \pm 0.1	1.6 \pm 0.2	62
SYK	0.25 \pm 0.12	1.3 \pm 0.2	1.6 \pm 0.3	0.38 \pm 0.10	1.0 \pm 0.2	1.3 \pm 0.2	0.16 \pm 0.11	1.2 \pm 0.1	1.5 \pm 0.2	37
TNKS2	0.37 \pm 0.09	1.0 \pm 0.2	1.2 \pm 0.2	0.45 \pm 0.10	0.9 \pm 0.1	1.1 \pm 0.2	0.41 \pm 0.10	0.8 \pm 0.1	1.0 \pm 0.1	45

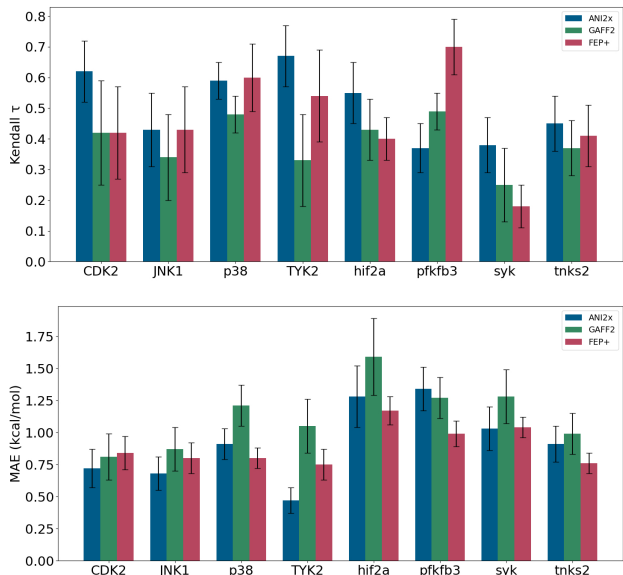


Figure 1: (Top) Kendall Tau and (bottom) Mean Absolute Error (MAE) for the $\Delta\Delta G$ s of each protein-ligand system calculated in combination with different force fields and reported estimates using FEP+¹⁶

low 1 kcal/mol. However, we acknowledge that the current NNP used in this study is limited to neutral molecules and a limited set of elements, posing a constraint on our exploration of the vast chemical space. Future endeavors should focus on expanding the applicability of NNPs to include charged ligands, thereby broadening the scope of our investigations. An increase in computing performance is also needed, probably with the inclusion of other integrators that allow for higher timesteps. Due to limited computational resources a random subset of all the possible calculations was computed. Although a potential bias could be included due to the nature of the subset we believe to have

a sampled an extensive number of data points to understand the capabilities of RBE along with the NNP/MM approach. Our work highlights the potential of NNP/MM for accurate RBE calculations and underscores the importance of further advancing NNPs to encompass a broader range of molecular species, and further improve the accuracy of these calculations.

5 Data and software availability

The calculated free energy values, ligand and protein structures, as well as preparation scripts, are available at https://github.com/compsciencelab/ATM_benchmark/tree/main/ATM_With_NNPs

6 Acknowledgement

The authors thank the volunteers of GPU-GRID.net for donating computing time. This project has received funding from the European Union’s Horizon 2020 research and innovation programme under grant agreement No. 823712; and the project PID2020-116564GB-I00 has been funded by MCIN / AEI / 10.13039/501100011033; the Torres-Quevedo Programme from the Spanish National Agency for Research (PTQ2020-011145 / AEI / 10.13039/501100011033). Research reported in this publication was supported by the National Institute of General Medical Sciences (NIGMS) of the National Institutes of Health under award number R01GM140090. E. G. acknowledges support from the United

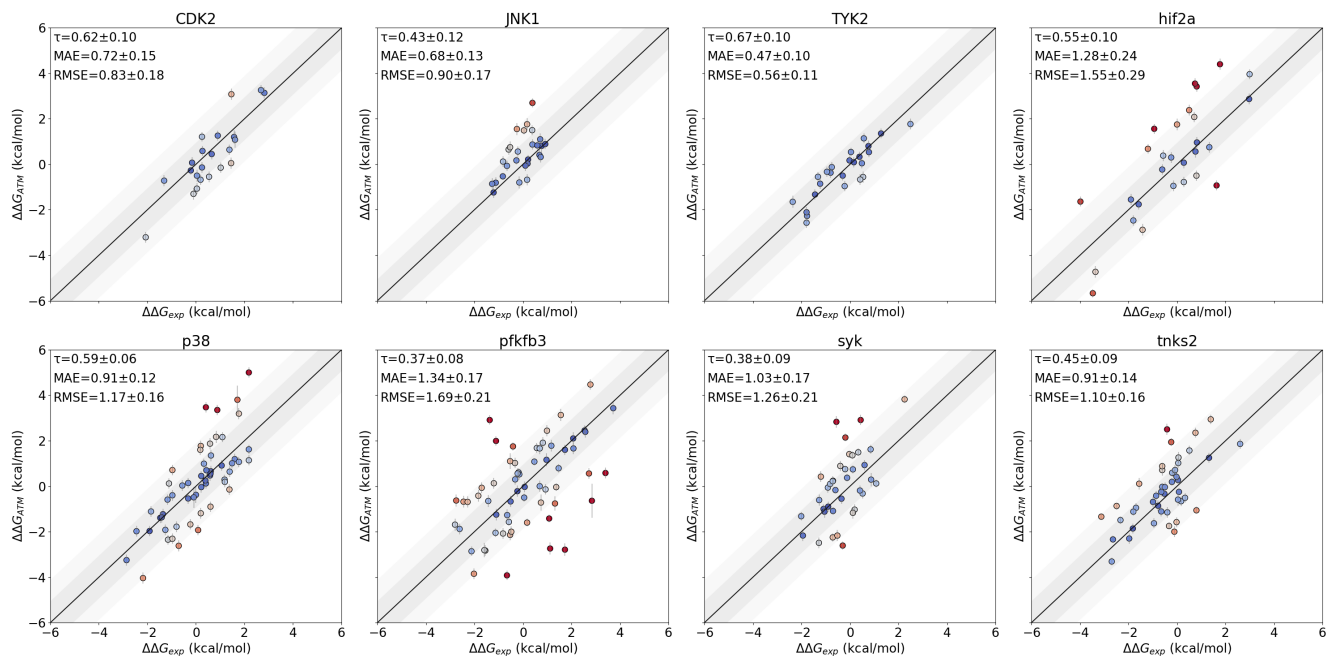


Figure 2: Performance in combination with the neural network potential (NNP) for each protein-ligand system studied. The calculated $\Delta\Delta G$ estimates are plotted against their corresponding experimental values. MAE and RMSE are in kcal/mol and τ is Kendall correlation.

States’ National Science Foundation (NSF CAREER 1750511). J.D.C. acknowledges support from NIH grant P30CA008748, R01GM140090, and the Sloan Kettering Institute. The content is solely the responsibility of the authors and does not necessarily represent the official views of the National Institutes of Health.

7 Associated Content

The Supporting Information contains: Description of the workflow used for this work. Barplots of the Pearson correlation and RMSE from the calculated versus experimental $\Delta\Delta G$ values for all systems and compared methods. Scatterplots for the calculated ΔG on all the connected systems and the comparison between the compared methods as well as barplots from the corresponding MAE, RMSE errors and R2 and Spearman correlations. Barplots with the analysis of the different speed performances between ATM and ATM combined with NNP/MM method. Scatterplots for a series of targets studied at different timesteps. Convergence analysis based on the estimation of the $\Delta\Delta G$ through simulated time.

8 Disclosures

J.D.C. is a current member of the Scientific Advisory Board of OpenEye Scientific Software, Redesign Science, Ventus Therapeutics, and Interline Therapeutics, and has equity interests in Redesign Science and Interline Therapeutics. The Chodera laboratory receives or has received funding from multiple sources, including the National Institutes of Health, the National Science Foundation, the Parker Institute for Cancer Immunotherapy, Relay Therapeutics, Entasis Therapeutics, Silicon Therapeutics, EMD Serono (Merck KGaA), AstraZeneca, Vir Biotechnology, Bayer, XtalPi, Interline Therapeutics, the Molecular Sciences Software Institute, the Starr Cancer Consortium, the Open Force Field Consortium, Cycle for Survival, a Louis V. Gerstner Young Investigator Award, and the Sloan Kettering Institute. A complete funding history for the Chodera lab can be found at <http://choderalab.org/funding>.

References

- (1) Wang, J.; Wolf, R. M.; Caldwell, J. W.; Kollman, P. A.; Case, D. A. Development and testing of a general amber force field. *Journal of computational chemistry* **2004**, *25*, 1157–1174.
- (2) Wang, J.; Wang, W.; Kollman, P. A.; Case, D. A. Automatic atom type and bond type perception in molecular mechanical calculations. *J. Mol. Graphics Modell.* **2006**, *25*, 247–260.
- (3) Vanommeslaeghe, K.; Hatcher, E.; Acharya, C.; Kundu, S.; Zhong, S.; Shim, J.; Darian, E.; Guvench, O.; Lopes, P.; Vorobyov, A., Igor MacKerell Jr CHARMM general force field: A force field for drug-like molecules compatible with the CHARMM all-atom additive biological force fields. *Journal of computational chemistry* **2010**, *31*, 671–690.
- (4) Vanommeslaeghe, K.; Raman, E. P.; MacKerell Jr, A. D. Automation of the CHARMM General Force Field (CGenFF) II: assignment of bonded parameters and partial atomic charges. *Journal of chemical information and modeling* **2012**, *52*, 3155–3168.
- (5) Roos, K.; Wu, C.; Damm, W.; Reboul, M.; Stevenson, J. M.; Lu, C.; Dahlgren, M. K.; Mondal, S.; Chen, W.; Wang, L.; Abel, R. OPLS3e: Extending force field coverage for drug-like small molecules. *Journal of chemical theory and computation* **2019**, *15*, 1863–1874.
- (6) Ponder, J. W.; Case, D. A. Force fields for protein simulations. *Advances in protein chemistry* **2003**, *66*, 27–85.
- (7) Dauber-Osguthorpe, P.; Hagler, A. T. Biomolecular force fields: where have we been, where are we now, where do we need to go and how do we get there? *Journal of computer-aided molecular design* **2019**, *33*, 133–203.
- (8) Hagler, A. T. Force field development phase II: Relaxation of physics-based criteria... or inclusion of more rigorous physics into the representation of molecular energetics. *Journal of computer-aided molecular design* **2019**, *33*, 205–264.
- (9) Beierlein, F. R.; Michel, J.; Essex, J. W. A simple QM/MM approach for capturing polarization effects in protein- ligand binding free energy calculations. *The Journal of Physical Chemistry B* **2011**, *115*, 4911–4926.
- (10) Devereux, C.; Smith, J. S.; Huddleston, K. K.; Barros, K.; Zubatyuk, R.; Isayev, O.; Roitberg, A. E. Extending the Applicability of the ANI Deep Learning Molecular Potential to Sulfur and Halogens. *Journal of Chemical Theory and Computation* **2020**, *16*, 4192–4202, PMID: 32543858.
- (11) Galvelis, R.; Varela-Rial, A.; Doerr, S.; Fino, R.; Eastman, P.; Markland, T. E.; Chodera, J. D.; De Fabritiis, G. NNP/MM: Accelerating molecular dynamics simulations with machine learning potentials and molecular mechanics. *Journal of chemical information and modeling* **2023**, *63*, 5701–5708.
- (12) Azimi, S.; Khuttan, S.; Wu, J. Z.; Pal, R. K.; Gallicchio, E. Relative binding free energy calculations for ligands with diverse scaffolds with the alchemical transfer method. *J. Chem. Inf. Model.* **2022**, *62*, 309–323.
- (13) Sabanés Zariquiey, F.; Pérez, A.; Majewski, M.; Gallicchio, E.; De Fabritiis, G. Validation of the Alchemical Transfer Method for the Estimation of Relative Binding Affinities of Molecular Series. *Journal of Chemical Information and Modeling* **2023**, *63*, 2438–2444, PMID: 37042797.

- (14) Chen, L.; Wu, Y.; Wu, C.; Silveira, A.; Sherman, W.; Xu, H.; Gallicchio, E. Performance and Analysis of the Alchemical Transfer Method for Binding Free Energy Predictions of Diverse Ligands. 2023.
- (15) Rufa, D. A.; Macdonald, H. E. B.; Fass, J.; Wieder, M.; Grinaway, P. B.; Roitberg, A. E.; Isayev, O.; Chodera, J. D. Towards chemical accuracy for alchemical free energy calculations with hybrid physics-based machine learning / molecular mechanics potentials. *bioRxiv* **2020**,
- (16) Wang, L.; Wu, Y.; Deng, Y.; Kim, B.; Pierce, L.; Krilov, G.; Lupyan, D.; Robinson, S.; Dahlgren, M. K.; Greenwood, J.; Romero, D. L.; Masse, C.; Knight, J. L.; Steinbrecher, T.; Beuming, T.; Damm, W.; Harder, E.; Sherman, W.; Brewer, M.; Wester, R.; Murcko, M.; Frye, L.; Farid, R.; Lin, T.; Mobley, D. L.; Jorgensen, W. L.; Berne, B. J.; Friesner, R. A.; Abel, R. Accurate and reliable prediction of relative ligand binding potency in prospective drug discovery by way of a modern free-energy calculation protocol and force field. *J. Am. Chem. Soc.* **2015**, *137*, 2695–2703.
- (17) Schindler, C. E. M.; Baumann, H.; Blum, A.; Böse, D.; Buchstaller, H.-P.; Burgdorf, L.; Cappel, D.; Chekler, E.; Czodrowski, P.; Dorsch, D.; Eguida, M. K. I.; Follows, B.; Fuchß, T.; Grädler, U.; Gunera, J.; Johnson, T.; Jorand Lebrun, C.; Karra, S.; Klein, M.; Knehans, T.; Koetzner, L.; Krier, M.; Leiendecker, M.; Leuthner, B.; Li, L.; Mochalkin, I.; Musil, D.; Neagu, C.; Rippmann, F.; Schiemann, K.; Schulz, R.; Steinbrecher, T.; Tanzer, E.-M.; Unzue Lopez, A.; Viacava Follis, A.; Wegener, A.; Kuhn, D. Large-Scale Assessment of Binding Free Energy Calculations in Active Drug Discovery Projects. *Journal of Chemical Information and Modeling* **2020**, *60*, 5457–5474, PMID: 32813975.
- (18) Galvelis, R.; Doerr, S.; Damas, J. M.; Harvey, M. J.; De Fabritiis, G. A scalable molecular force field parameterization method based on density functional theory and quantum-level machine learning. *Journal of chemical information and modeling* **2019**, *59*, 3485–3493.
- (19) Doerr, S.; Harvey, M.; Noé, F.; De Fabritiis, G. HTMD: high-throughput molecular dynamics for molecular discovery. *Journal of chemical theory and computation* **2016**, *12*, 1845–1852.
- (20) Zou, J.; Tian, C.; Simmerling, C. Blinded prediction of protein–ligand binding affinity using Amber thermodynamic integration for the 2018 D3R grand challenge 4. *J. Comput.-Aided Mol. Des.* **2019**, *33*, 1021–1029.
- (21) Maier, J. A.; Martinez, C.; Kasavajhala, K.; Wickstrom, L.; Hauser, K. E.; Simmerling, C. ff14SB: improving the accuracy of protein side chain and backbone parameters from ff99SB. *J. Chem. Theory Comput.* **2015**, *11*, 3696–3713.
- (22) openmm sdm plugin. https://github.com/Gallicchio-Lab/openmm_sdm_plugin, [Accessed 12-12-2023].
- (23) Gallicchio, E.; Xia, J.; Flynn, W. F.; Zhang, B.; Samlalsingh, S.; Menten, A.; Levy, R. M. Asynchronous replica exchange software for grid and heterogeneous computing. *Comput. Phys. Commun.* **2015**, *196*, 236–246.
- (24) AToM-OpenMM. <https://github.com/Gallicchio-Lab/AToM-OpenMM>, [Accessed 12-12-2023].
- (25) Tan, Z.; Gallicchio, E.; Lapelosa, M.; Levy, R. M. Theory of binless multi-state free energy estimation with applications to protein-ligand binding. *The Journal of Chemical Physics* **2012**, *136*, 04B608.

- (26) Macdonald, H. B.; dfhahn,; Henry, M.; Chodera, J.; Dotson, D.; Glass, W.; Pulido, I. openforcefield/openff-arsenic: v0.2.1. 2022; <https://doi.org/10.5281/zenodo.6210305>.
- (27) Hahn, D. F.; Bayly, C. I.; Bobby, M. L.; Macdonald, H. E. B.; Chodera, J. D.; Gapsys, V.; Mey, A. S.; Mobley, D. L.; Benito, L. P.; Schindler, C. E.; Tresadern, G.; Warren, G. L. Best practices for constructing, preparing, and evaluating protein-ligand binding affinity benchmarks [article v1. 0]. *Living journal of computational molecular science* **2022**, *4*.

9 Supporting Information

Supporting Methods

Table S1: Percentage of predictions that have a MAE lower than 1 or 1.5 kcal/mol for each system.

Protein	GAFF2		NNP/MM ANI2x		FEP+	
	% MAE < 1	% MAE < 1.5	% MAE < 1	% MAE < 1.5	% MAE < 1	% MAE < 1.5
CDK2	54.6 ± 4.9	71.1 ± 4.5	64.0 ± 9.3	96.0 ± 3.9	54.5 ± 10.3	86.4 ± 7.2
JNK1	54.9 ± 4.7	79.6 ± 3.7	74.1 ± 8.3	88.9 ± 6.0	70.4 ± 8.9	85.2 ± 6.8
p38	49.9 ± 2.5	65.4 ± 2.4	55.9 ± 6.2	81.4 ± 5.0	64.3 ± 6.3	83.9 ± 4.8
TYK2	48.0 ± 3.6	68.4 ± 3.3	85.0 ± 5.6	97.5 ± 2.5	87.5 ± 7.9	87.5 ± 7.9
hif2a	36.0 ± 4.6	55.9 ± 4.9	41.9 ± 8.6	58.1 ± 8.8	55.2 ± 8.9	75.9 ± 8.1
pfkfb3	41.8 ± 3.6	60.4 ± 3.6	42.9 ± 6.2	65.1 ± 6.2	61.3 ± 6.1	80.6 ± 5.1
syk	40.4 ± 4.6	61.4 ± 4.6	59.5 ± 8.0	78.4 ± 6.8	42.1 ± 8.0	73.7 ± 7.1
tnks2	55.8 ± 5.2	70.5 ± 4.7	66.7 ± 7.1	77.8 ± 6.3	75.6 ± 6.2	88.9 ± 4.2



Step #1

Receptor
Ligand A + Ligand B

Parameterize



Step #2

Complex system set-up
Move Ligand B based on vector

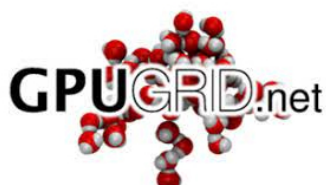
HTMD



Step #3

Energy minimisation and equilibration
Annealing at $\lambda = 1/2$ and equilibration

OpenMM



Step #4

Free energy calculations
Asynchronous Replica Exchange
22 x ≈ 3 ns per λ

OpenMM

Step #5

Results analysis

UWHAM

Figure S1: The ATM workflow used in this work. Ligands topologies are calculated with *parameterize* with GAFF2 and Sage force fields. (2) System complexes are prepared and built with *htmd*¹⁹. Protein topologies are prepared with the Amber ff14SB force field. Next ligand B is displaced based on a vector. (3) Energy minimization and equilibration is performed. Later an annealing and equilibration at $\lambda=1/2$ is performed. (4) Replica Exchange simulations are performed for a total sampling of 60ns. ATM simulations were run in GPU GRID were as ATM-NNP calculations were performed in our local cluster.(5) After the simulations were finished, these were analyzed with the UWHAM package to obtain the calculated $\Delta\Delta G$ estimates.

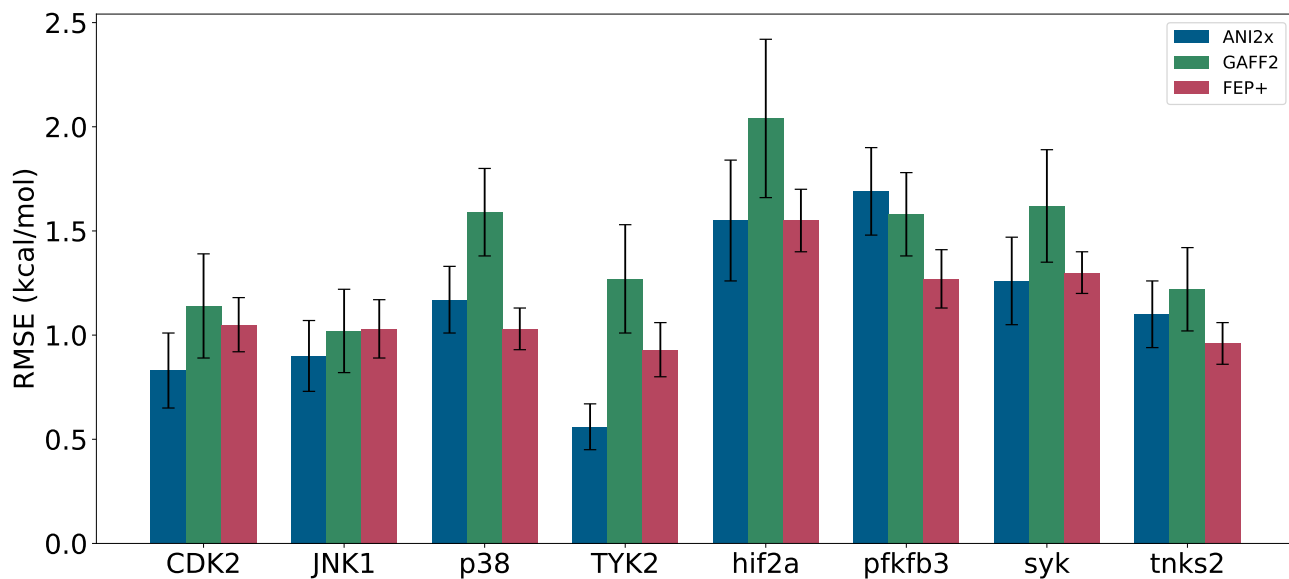


Figure S2: Pearson correlation for each protein-ligand system calculated in combination with different force fields and reported estimates using FEP+

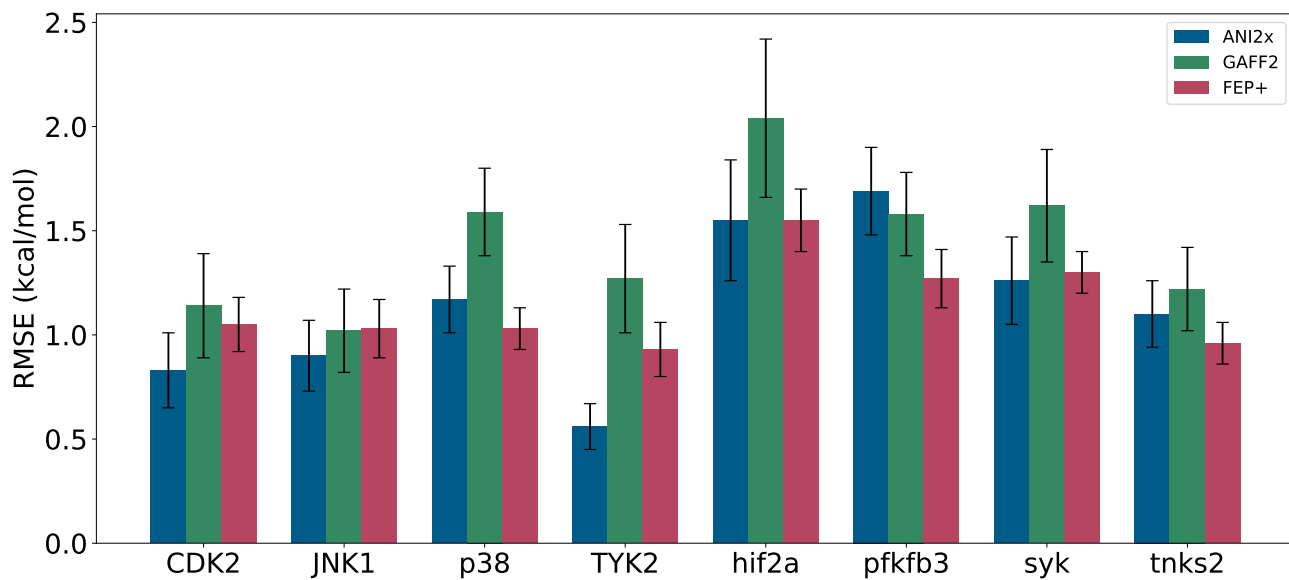


Figure S3: Root Mean Square Error (RMSE) in kcal/mol for each protein-ligand system calculated in combination with different force fields and reported estimates using FEP+

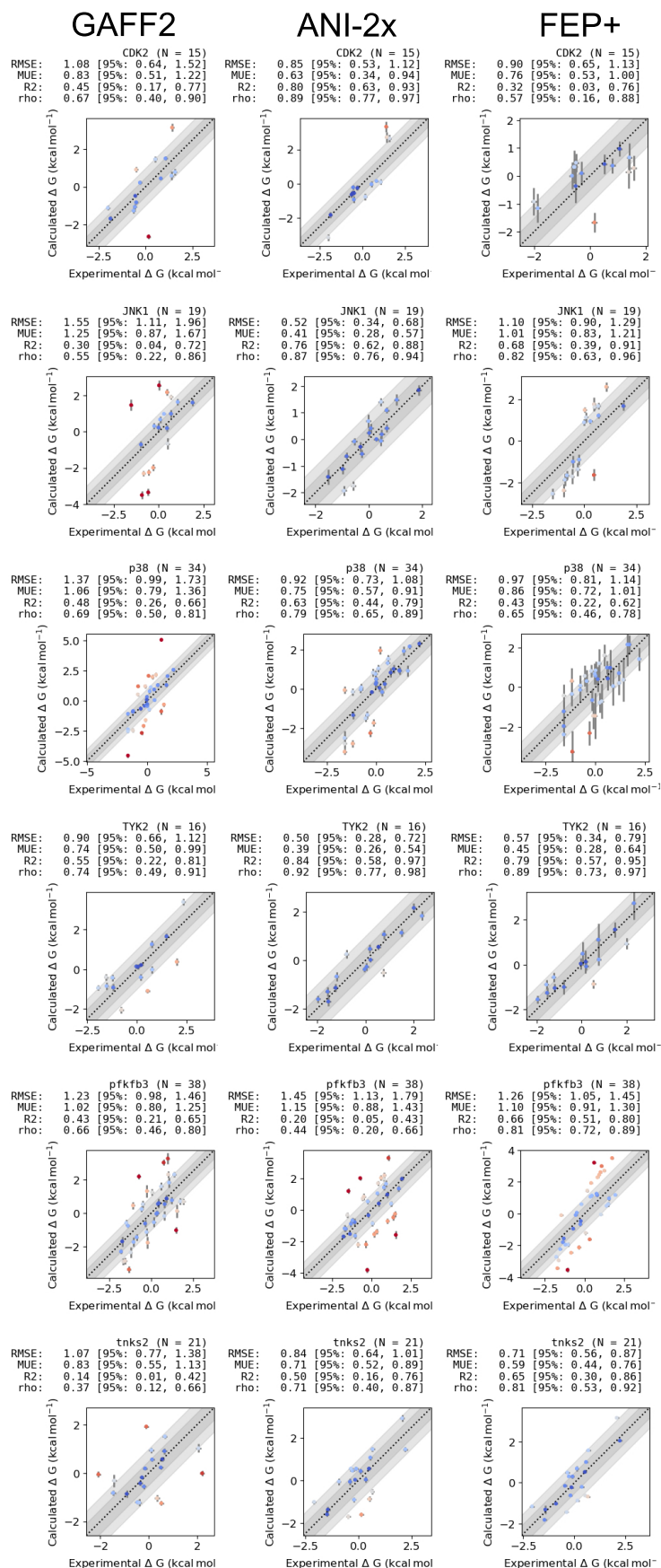


Figure S4: Scatterplots for the ΔG calculated on all the connected systems. Comparison between GAFF2, NNP/MM and FEP+.

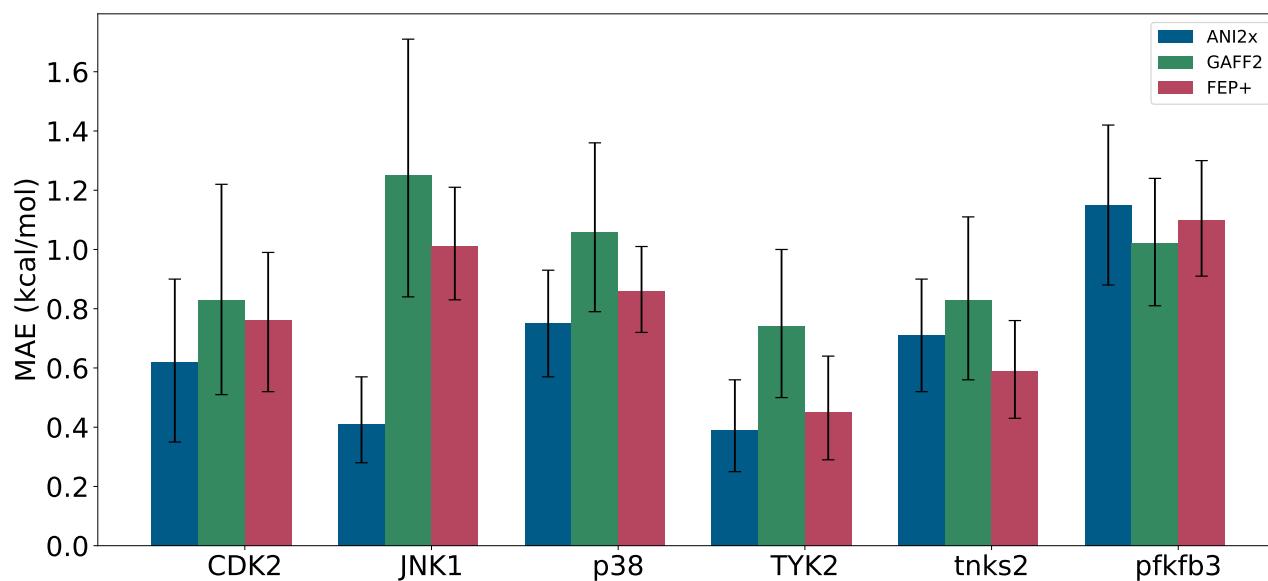


Figure S5: MAE (kcal/mol) for the ΔG values on all the connected systems

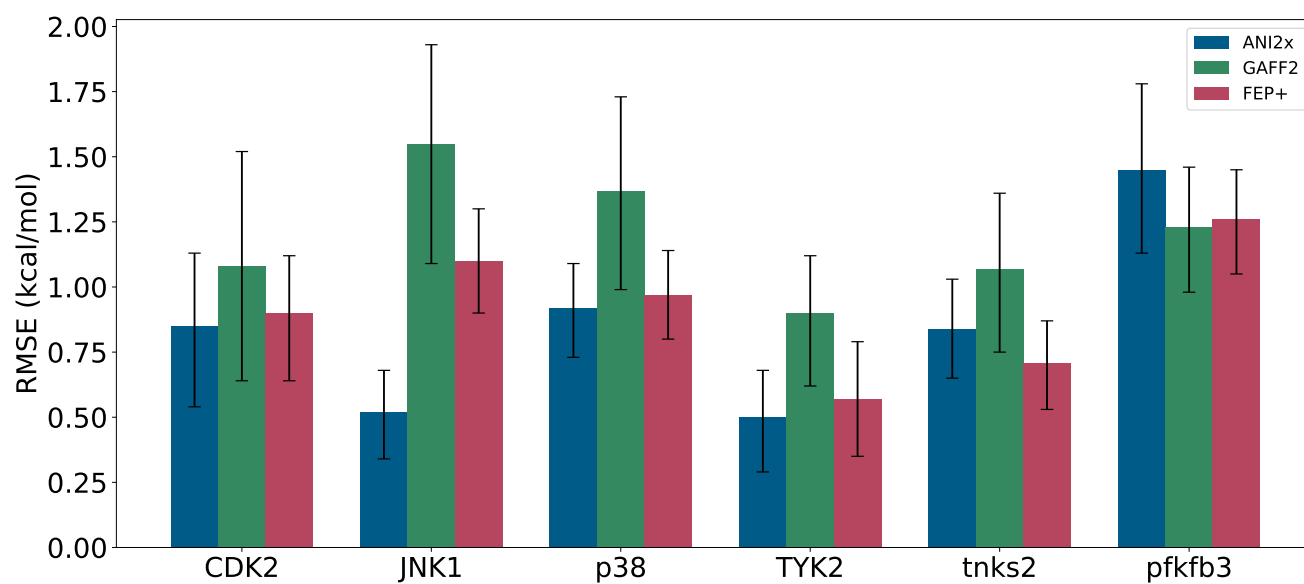


Figure S6: RMSE (kcal/mol) for the ΔG values on all the connected systems

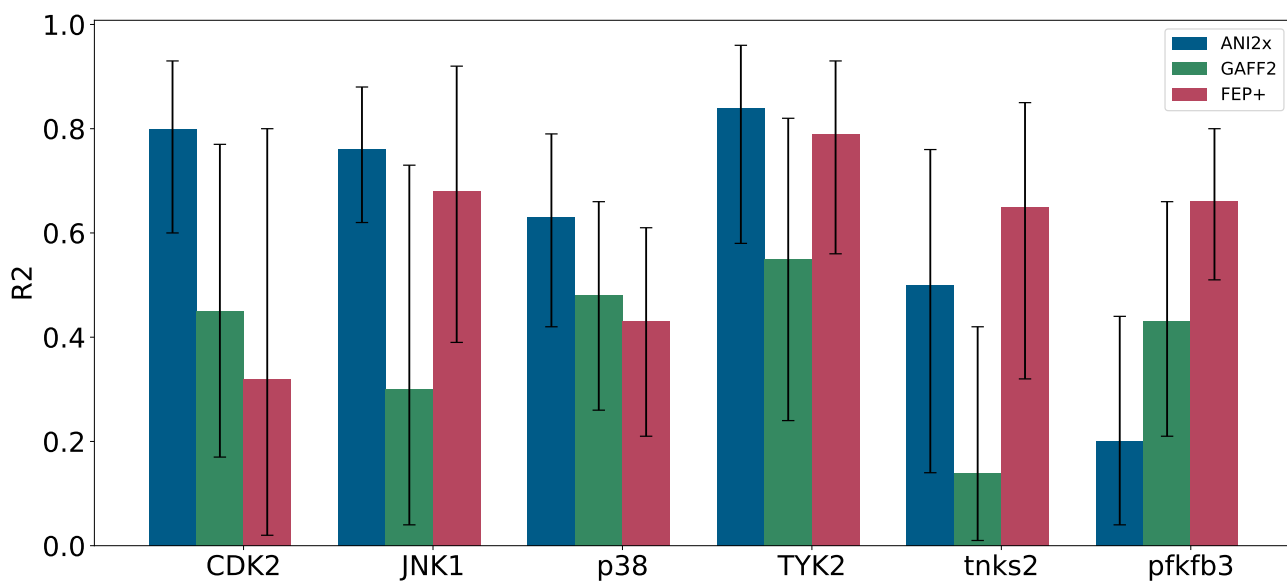


Figure S7: R2 correlation for the ΔG values on all the connected systems

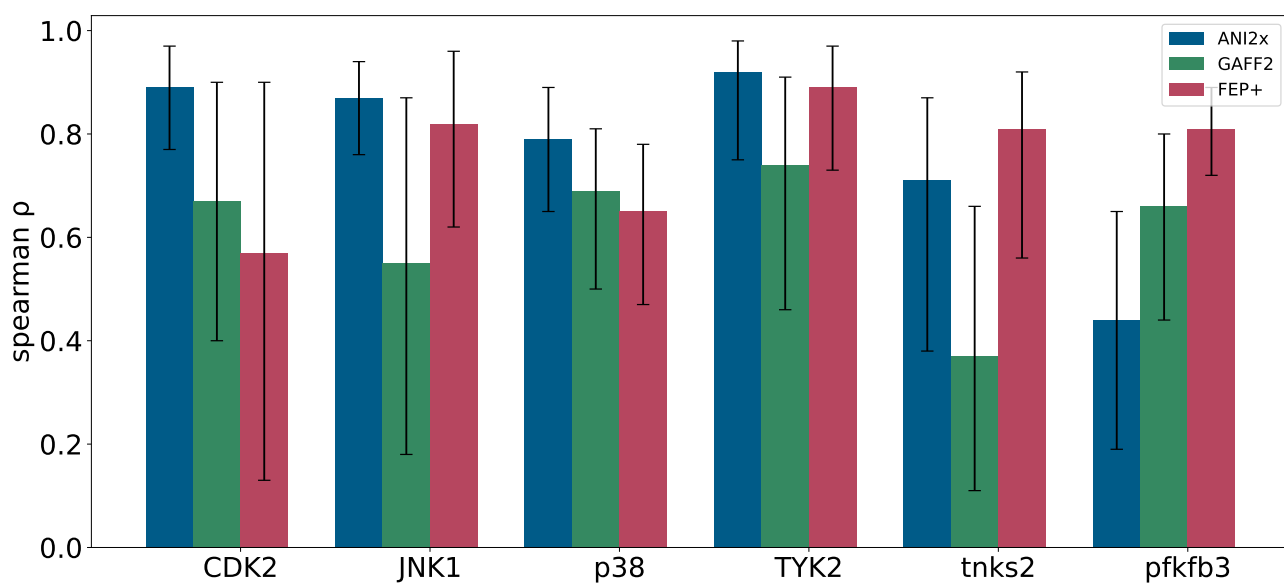


Figure S8: Spearman correlation for the ΔG values on all the connected systems

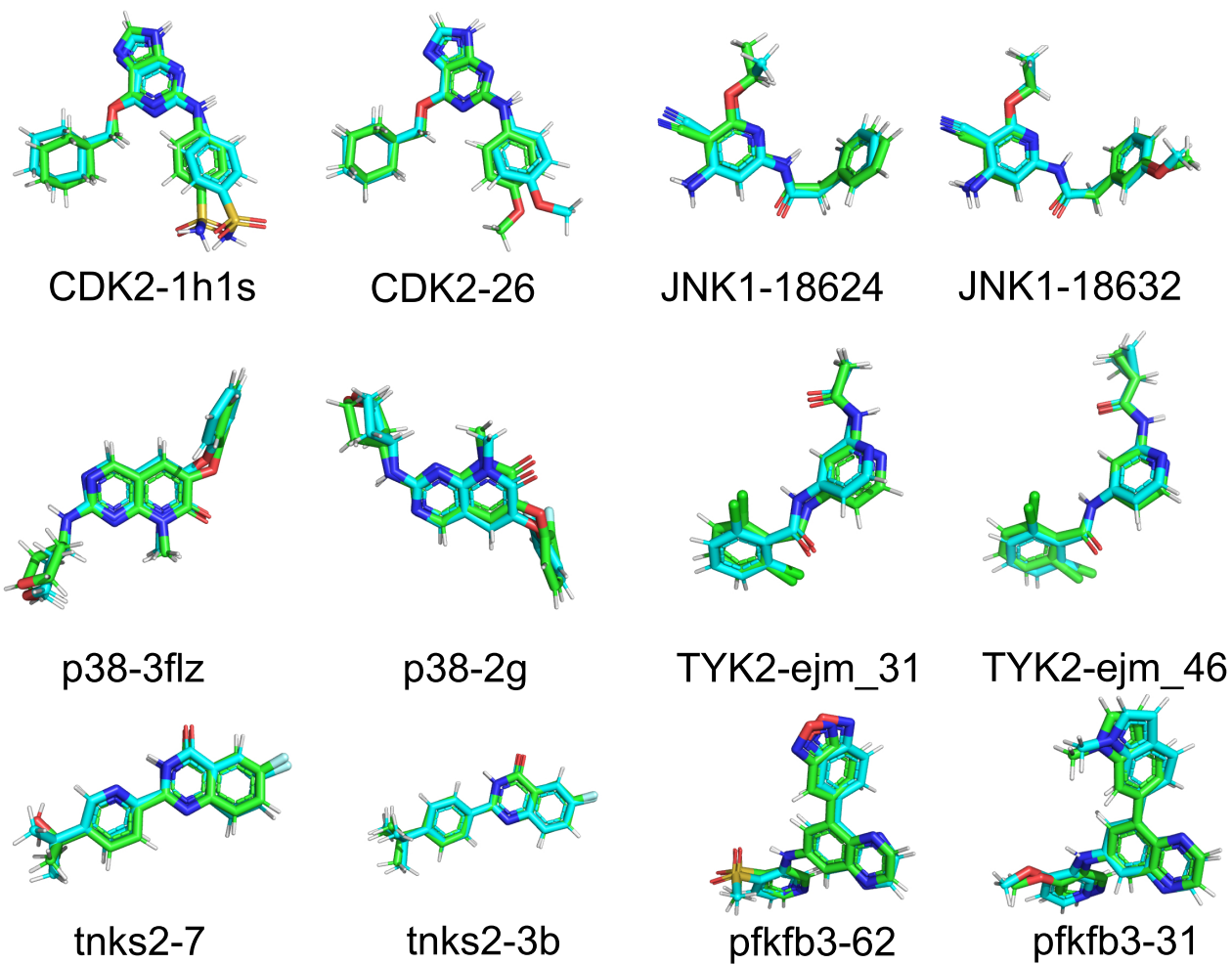


Figure S9: Generated conformers after equilibration for runs performed with GAFF2 (cyan) and ANI-2x (green).

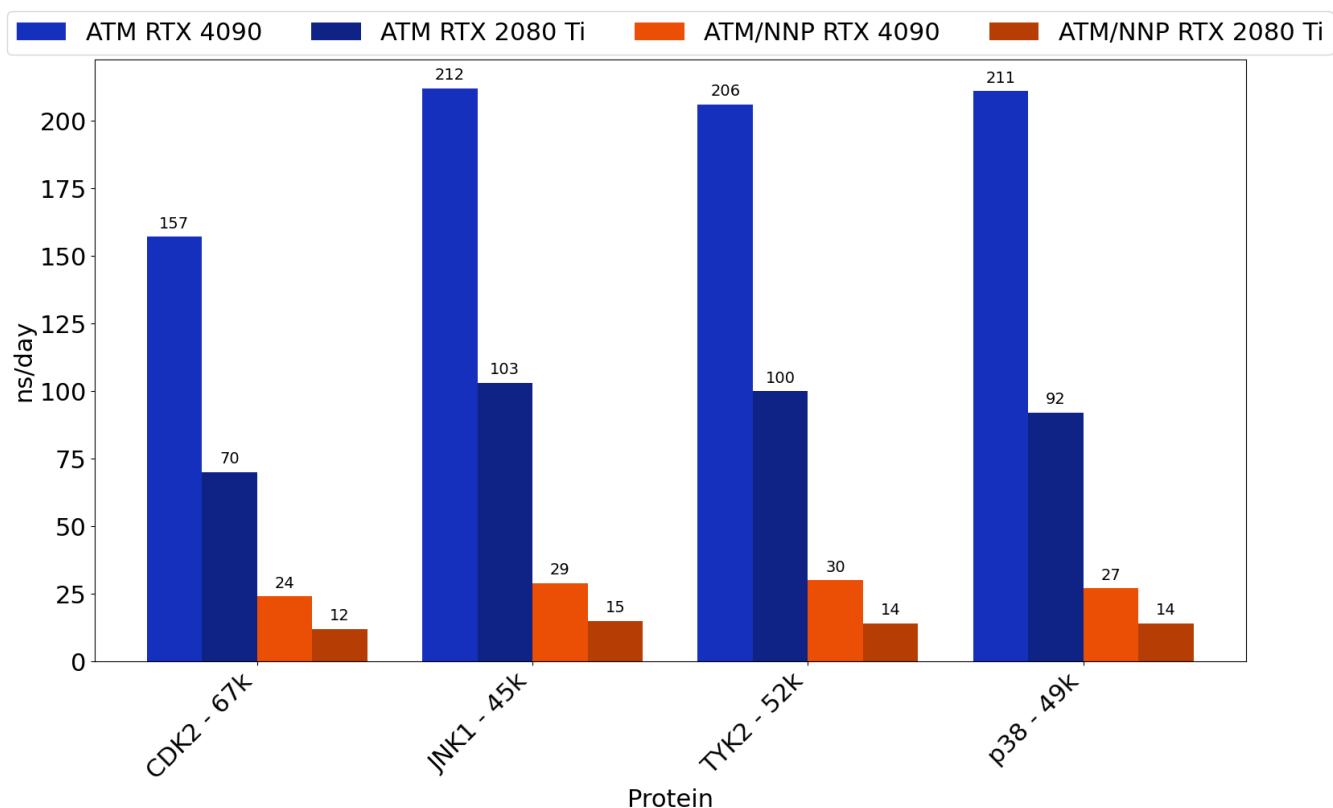


Figure S10: Performance of ATM and ATM/NNP on RTX 2080Ti and RTX 4090 graphics cards with OpenMM 7.7 MD engine and the ATM Meta Force plugin using the CUDA platform

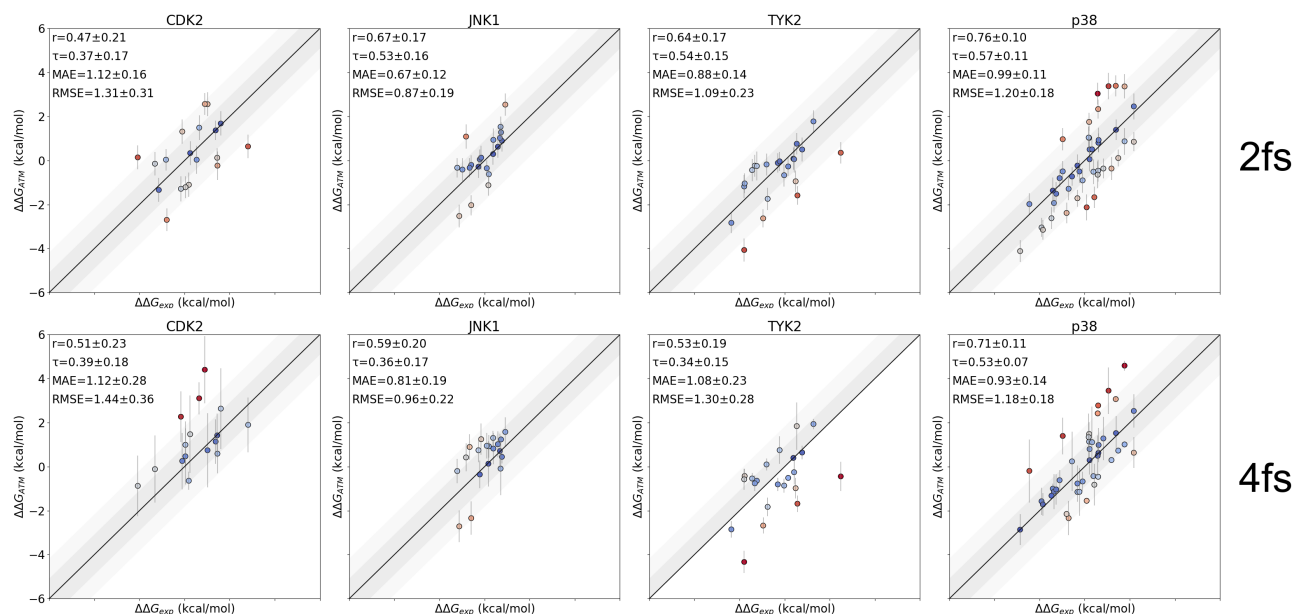


Figure S11: Scatterplots for a series of targets studied at different timesteps. Top row are the relevant ligand pairs studied in our previous work, which we realized with a 2fs timestep. Bottom row are the calculations done for these targets at a 4fs timestep.

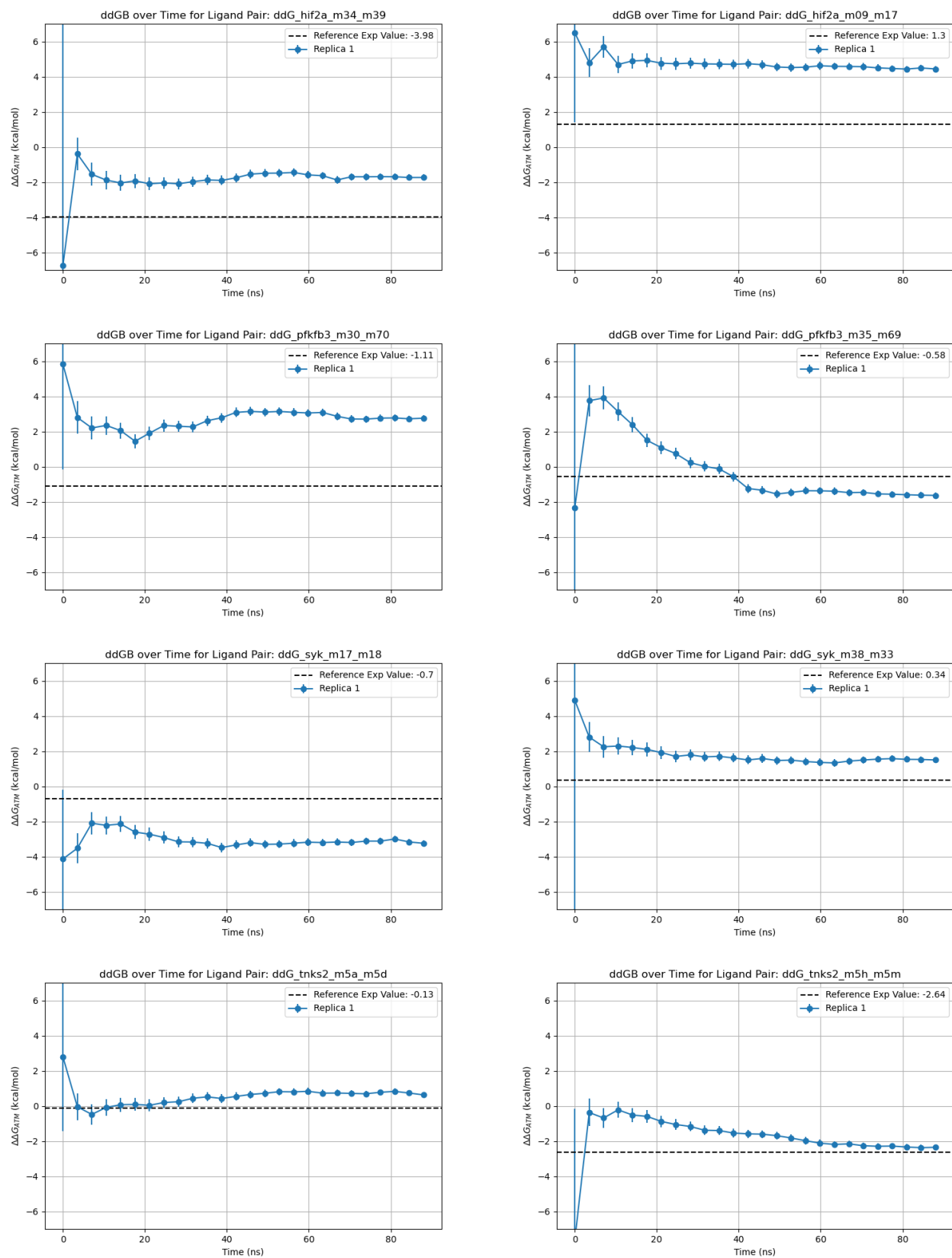


Figure S12: Free energy convergence as a function of time for a series of ligand pairs of hif2a, pfkfb3, syk and tnks2

Table S2: Case study example of the $\Delta\Delta G$ s obtained with NNP/MM and GAFF2. We observe how the transformations with the ligand ejm_55 give poor results with the GAFF2 (highlighted red) calculations but in the case of NNP/MM (highlighted green) the MAE is below 1kcal/mol.

Protein: TYK2			NNP/MM ANI2x			GAFF2		
ligand1	ligand2	exp_ddG	ATM_ddG	error	MAE	ATM_ddG	error	MAE
ejm_31	ejm_46	-1.77	-2.27	0.25	0.50	-0.42	0.24	1.35
ejm_31	ejm_43	1.28	1.36	0.22	0.07	1.94	0.23	0.66
ejm_31	jmc_28	-1.44	-1.33	0.22	0.11	-0.54	0.23	0.90
ejm_31	ejm_45	-0.02	0.17	0.23	0.19	-0.86	0.23	0.84
ejm_31	ejm_48	0.54	-0.56	0.24	1.10	1.84	0.24	1.30
ejm_50	ejm_42	-0.80	-0.37	0.22	0.43	0.10	0.22	0.90
ejm_55	ejm_54	-1.32	-0.55	0.22	0.77	-0.76	0.23	0.56
ejm_43	ejm_55	-0.95	-0.33	0.23	0.62	-2.68	0.23	1.73
jmc_28	jmc_30	0.04	0.57	0.26	0.53	-1.07	0.28	1.11
jmc_28	jmc_27	-0.30	-0.50	0.22	0.20	-0.80	0.22	0.50
ejm_49	ejm_31	-1.79	-2.57	0.24	0.78	-0.57	0.24	1.22
ejm_49	ejm_50	-1.23	-0.86	0.24	0.38	-0.64	0.24	0.59
ejm_45	ejm_42	-0.22	-0.96	0.22	0.74	0.75	0.23	0.97
ejm_44	ejm_55	-1.79	-2.11	0.24	0.32	-4.33	0.23	2.54
ejm_44	ejm_42	-2.36	-1.65	0.27	0.71	-2.85	0.24	0.49
ejm_47	ejm_31	0.16	0.09	0.22	0.07	-0.51	0.23	0.67
ejm_47	ejm_55	0.49	0.04	0.22	0.44	-0.98	0.23	1.47
jmc_23	jmc_30	0.76	0.87	0.27	0.11	-0.25	0.25	1.01
jmc_23	ejm_46	0.39	0.33	0.22	0.06	0.40	0.22	0.01
jmc_23	ejm_55	2.49	1.77	0.23	0.72	-0.44	0.23	2.93
jmc_23	jmc_27	0.42	-0.67	0.24	1.09	-0.25	0.22	0.67
ejm_42	ejm_55	0.57	1.14	0.22	0.57	-1.68	0.22	2.25
ejm_42	ejm_48	0.78	0.53	0.22	0.25	0.64	0.23	0.14
ejm_42	ejm_54	-0.75	-0.12	0.22	0.62	-1.83	0.22	1.08

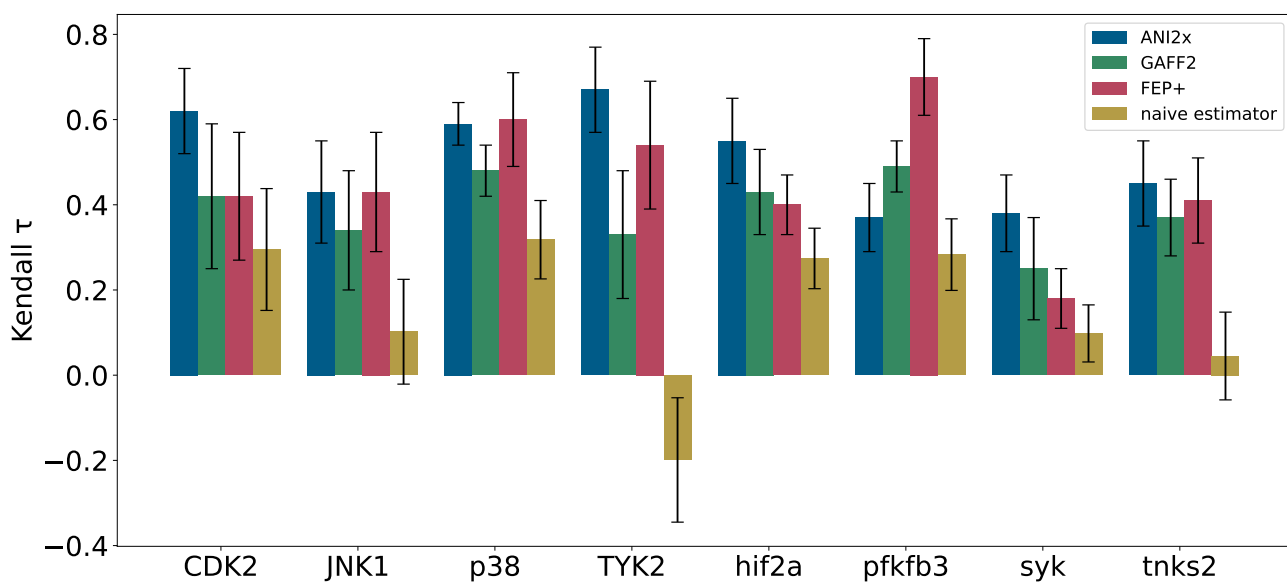


Figure S13: Comparison of Kendall tau for the $\Delta\Delta G$ s of each protein-ligand system calculated and compared against a naive estimator based on the difference of molecular weight between ligands